Imaging subduction, collision, and extension in northern Borneo: Constraints from receiver functions

Amy Gilligan(1),* David G. Cornwell(1), Nicholas Rawllinson(2), Felix Tongkul(3), Simone Pilia(4), Tim Greenfield(2), Conor Bacon(5)

1. *School of Geosciences, University of Aberdeen, Aberdeen, UK*
2. *Department of Earth Sciences, University of Cambridge, Cambridge, UK*
3. *Faculty of Science and Natural Resources, Universiti Malaysia Sabah, Kota Kinabalu, Malaysia*
4. *College of Petroleum Engineering and Geosciences, King Fahd University of Petroleum and Minerals, Dhahran, Saudi Arabia*
5. *Lamont-Doherty Earth Observatory, Columbia University, Palisades, New York, USA*

** Corresponding author: amy.gilligan@abdn.ac.uk, @seismo_amy*

Imaging subduction, collision, and extension in northern Borneo: Constraints from receiver functions

Amy Gilligan(1),* David G. Cornwell(1), Nicholas Rawllinson(2), Felix Tongkul(3), Simone Pilia(4), Tim Greenfield(2), Conor Bacon(5)

6. *School of Geosciences, University of Aberdeen, Aberdeen, UK*
7. *Department of Earth Sciences, University of Cambridge, Cambridge, UK*
8. *Faculty of Science and Natural Resources, Universiti Malaysia Sabah, Kota Kinabalu, Malaysia*
9. *College of Petroleum Engineering and Geosciences, King Fahd University of Petroleum and Minerals, Dhahran, Saudi Arabia*
10. *Lamont-Doherty Earth Observatory, Columbia University, Palisades, New York, USA*

** Corresponding author: amy.gilligan@abdn.ac.uk*

Summary

Northern Borneo (Sabah) has a complex geological history, having experienced multiple episodes of subduction, magmatism, uplift, subsidence, and extension since the Mesozoic. This includes the subduction of the proto-South China Sea beneath what is now the northwestern margin of Sabah, which terminated ~21 Ma; a postulated later phase of northward subduction of the Celebes Sea plate, which terminated ~9 Ma; extension in central Sabah ~9-10Ma; rapid emplacement and exhumation of a granite intrusion ~7Ma, which forms Mt Kinabalu today, and the development of a fold and thrust belt offshore during the last 5 Myr. While these events have all left an imprint in the rock record at the surface, it has not been possible, until recently, to investigate deeper lithospheric processes that have shaped Sabah. However, the installation of 46 broadband seismometers with an ~40 km station spacing as part of the northern Borneo Orogeny Seismic Survey (nBOSS) between

2018 and 2020, means that for the first time it is now possible to constrain the architecture of the crust and uppermost mantle beneath Sabah. Here we present the results of receiver function analysis using two years of passive seismic data recorded by the nBOSS network, and an additional 24 Malaysian Metrological Service broadband seismometers also located in Sabah. We calculate P-wave receiver functions and use these in a joint inversion with surface wave data to obtain shear velocity models of crustal structure. We find that the crustal thickness in northern Borneo varies between 22 and 60 km. The thickest crust occurs beneath the Crocker Range, while the thinnest crust is found in central Sabah, potentially recording Miocene extension. The crust beneath the 4095m high Mt Kinabalu is also comparatively thin. Distinct, low velocity, dipping anomalies identified in our shear wave velocity models provide clear evidence for underthrusting of Dangerous Grounds continental crust following subduction and collision.

Keywords

Asia; Crustal Structure; Crustal Imaging; Subduction Zone Processes; Joint Inversion

Introduction

Subduction is fundamental to the growth of continents (e.g. Foley et al., 2002), driving plate motion (Forsyth and Uyeda, 1975), and long-term climate regulation (e.g. Johnston et al., 2011). Eventually subduction will come to an end (e.g., via continent-continent collision), and this may result in magmatism, exhumation, rapid uplift, and subsidence (e.g. Zandt et al., 2004, Levander et al., 2011, Li et al., 2016). The processes occurring in these post-subduction settings remain, at present, poorly understood. Given that subduction has been happening on Earth for at least 1.8 Ga (Weller and St Onge, 2017), explaining post-subduction processes is vital, not just for our understanding of present-day tectonics, but also for interpreting the deep geological record.

Northern Borneo is an ideal location for studying post-subduction processes. It is thought to be the site of two subduction systems that have terminated since the start of the Neogene: the subduction of the proto-South China Sea (pSCS) until ~21 Ma (Lai et al., 2021 , Hall 2013, Morley and Back, 2008, Tongkul 1994, Tongkul 1991) along the present-day NW coast of Sabah, and the subduction of the Celebes Sea along the present-day SE coast of Sabah, which terminated ~9 Ma (Lai et al., 2021). In this study we use passive seismic data recorded by a network of broadband seismometers deployed across the Malaysian state of Sabah, situated on the northern end of the island of Borneo, between 2018-2020 (Figure 1) to image the crust and mantle lithosphere to both improve our understanding of the tectonic setting of northern Borneo and provide new insight into subduction termination and post-subduction processes.

Geology and tectonic setting of Sabah

The diverse surface geology of Sabah is testament to the rich range of tectonic processes that have affected the northern part of Borneo since the Mesozoic. The oldest dated rocks are those of the Segama Valley Felsic

Intrusions (250 and 241 Ma) (Burton-Johnson et al., 2020) in eastern Sabah, which are intruded into ophitic rocks, with some subsequent, mineralogically distinct, felsic intrusions in the same area being dated at ~178 Ma. It has been proposed (Burton-Johnson et al. 2020, Balaguru and Nichols, 2004) that these formed in an extensional basin in a suprasubduction setting, which was then uplifted and eroded in the latest Cretaceous or earliest Paleocene, around 66 Ma (Balaguru and Nichols, 2004).

By the Paleocene (66-56Ma) subduction of the proto-South China Sea towards the south-east beneath what is now the western edge of Sabah had begun (e.g., Hutchison et al., 2000, Rangin et al., 1999). Cumulate gabbros, part of the Sabah Ophiolite, in the Tongod-Telupid area have been dated to 42.65 ± 0.51 Ma (Lai et al., 2021), and from their geochemical signature are thought to have formed in a back-arc basin. Similarly, the geochemistry of the Sandakan andesitic tuff (33.9 ± 7.7 Ma, Bergman et al., 2000) could also suggest a back arc basin setting (Lai et al., 2021, Hutchison et al., 2000). In the fore-arc, thick (~9000 m) sedimentary successions of deep marine sandstones, shales and minor conglomerates, are present in the NE-SW trending Crocker Basin (Balaguru and Nichols, 2004).

Opening of the South China Sea (~33-32 Ma, (Franke, 2013, Barckhausen et al., 2014, Li et al., 2014)), driven by subduction of the proto-South China Sea, pushed continental slivers, including the Dangerous Grounds and Reed Bank blocks, towards Borneo (e.g. Tongkul 1991, Tongkul 1994, Hutchison et al., 2000, Hall 2013, Rangin et al., 1999). Subduction of the proto-South China

Sea continued in the earliest part of the Miocene (24-21 Ma, Lai et al., 2021 and references therein), however, at around 21 Ma the Dangerous Grounds block collided with and then underthrust northern Borneo (Lai et al., 2021, Hall 2013, Morley and Back, 2008, Tongkul 1994, Tongkul 1991), which ultimately caused subduction to cease. This collision led to uplift above sea level (Burton-Johnson et al, 2020, Hall 2013, Morley and Back, 2008). However, by the end of the Early Miocene, most of Sabah was at or below sea level once more, with low hills where the Crocker Range is today (Hall 2013, Cottam et al, 2013).

Subduction of the Celebes Sea beneath eastern Sabah began at a similar time to the termination of subduction of the proto-South China Sea and may have been a result of changes in regional stresses due to the Sabah-Dangerous Grounds collision (Lai et al., 2021, Linang et al., 2022). In the Dent Peninsular, rocks that are the product of arc magmatism have been dated to 18.8-17.8 Ma and in the Semporna Peninuslar to 18.2-14.4 Ma (Macpherson et al., 2010). It is, however, important to note that the idea that there was northwards subduction of the Celebes Sea is contested (Burton-Johnson and Cullen, 2023). A slab from this subduction event has yet to be imaged in the mantle.

Roll-back of the Celebes Sea subduction from 19 Ma led to extension in the Sulu Sea and in Sabah (Hall, 2013). Thick (~6 km) successions of carbonates, shallow marine, and fluvio-deltaic sediments, including coals, were deposited in a basin in Central Sabah (Tongkul and Chang, 2003, Balaguru and Nichols 2004, Burton-Johnson et al., 2021). The coastal/shelf environments for all these sediments, including coal that was buried to 3 km depth (Baluguru and Nichols, 2004), means that subsidence must have continued over a prolonged period. Tsikouras et al., (2021) argue that the major increase in extension suggested by Huang (1991) between 9 and 11 Ma lead to rifting in Ranau area, and suggest that sea-floor spreading took place in the Telupid area. This is disputed by Cullen and Burton-Johnson (2021) who argue that while extension took place, the Sulu sea rift did not extend into Sabah. In a recent review Lai et al., (2021) suggest that Celebes Sea subduction beneath Borneo terminated ~9 Ma.

The Kinabalu pluton, which forms the 4095 m high Mt Kinabalu, was intruded into peridotites and the Crocker formation between 7.85 and 7.22 Ma, at a depth of 3-8 km (Cottam et al., 2013). Between 6.6 and 5.8 Ma it was rapidly cooled and exhumed with rates of up to 7 mm/yr (Cottam et al., 2013). The emplacement and exhumation of the Kinabalu pluton likely occurred in an extensional setting (Hall et al., 2013, Burton-Johnson et al., 2019).

Sabah only became fully emergent above sea level by the end of the Miocene to early Pliocene (~5 Ma), and uplift has occurred since (Roberts et al., 2018, Hall 2013, Morley and Black 2008). This includes uplift of the circular basins, such as the Maliau Basin, in central Sabah (Tongkul and Chang, 2003). During the Pliocene large-scale gravitational collapse occurred, seen in mass transport slumps, megaslides and extensional faults (Cottam et al., 2013), and as result of this, a fold and thrust belt has developed offshore of western

Sabah (e.g., Spain et al., 2013, Franke et al., 2008, King et al., 2010). Around 5 Ma a change in the composition of volcanic rocks in eastern Sabah also occurs from calc-alkaline to a similar composition to ocean island basalts (OIB), (Macpherson et al., 2010). Volcanism in eastern Sabah has continued into the Holocene, potentially as recently as 24-27 ka dated from radiocarbon dating of carbonised material (Kirk, 1968; Bellwood, 1988; cited in Tjia et al., 1992), although Takashima et al., (2004) date the youngest volcanics in their study using thermo-luminescence to 90ka.

Previous geophysical work

Regional-scale tomographic studies of South-East Asia have observed anomalously high seismic velocities in the upper mantle beneath Sabah at depths of ~100-300 km (e.g. Amaru, 2007, Tang and Zheng, 2013, Hall and Spakman, 2015, Zenonos et al., 2019, Wehner et al., 2022). These high velocities are attributed to the presence of slab remnants in the upper mantle. While the earlier body-wave studies (e.g., Amaru, 2007, Hall and Spakman 2015, Zenonos et al., 2019) had limited resolution beneath Sabah, thus bringing the existence of higher velocities into question, the full-waveform model of Wehner et al., (2022), SASSY21, uses data from the same dense seismic network in Borneo used in this study, and so has improved resolution in this region. Other results from this dense seismic network – the nBOSS network – are described below.

In a Sabah-focused P- and S-wave tomographic study, also using nBOSS data, Pilia et al., (2023a), observe two distinct fast velocity anomalies in the upper mantle beneath Sabah. One, an elongate anomaly at depths >250 km underlying most of the Crocker Range, is attributed to the proto-South China Sea Slab, while the other, a relatively narrow (<100 km) anomaly between ~150 and 300 km depth in central Sabah, is interpreted to be a lithospheric drip from beneath the Semporna Peninsular. Pilia et al., (2023b) perform thermo-mechanical modelling and suggest that the downwelling drip can cause extension and crustal thinning, resulting in melting and exhumation of sub continental material. As such, the ‘Semporna drip’ may play an important role in the emplacement of the Kinabalu pluton, as well as explaining subsidence and uplift, and the lavas with an OIB composition in eastern Sabah.

Bacon et al., (2022) investigate anisotropy beneath Sabah using XKS splitting measurements extracted from nBOSS teleseismic data. Their results demonstrate that fossil anisotropy in the lithosphere is the main control on anisotropic properties in this post-subduction setting. They observe fast directions parallel to the strike of the Crocker range in western Sabah, likely imparted when the Dangerous Grounds block collided with Sabah. In the east of Sabah, fast directions are sub-parallel to the direction of spreading in the Sulu Sea, suggesting that the anisotropic fabric may have developed as a result of extension, while the null results they observe in the southeast may arise due to the lithospheric drip observed by Pilia et al., (2023a).

Roberts et al., (2018) suggest that removal of the lithosphere and replacement by hot asthenospheric material could explain the relatively rapid uplift and erosion rates observed in Sabah (~0.1-0.3 mm/yr, Morely and Back, 2008). They base their estimates of thin lithosphere on regionally extensive slow shear wave velocities at 100-200 km depth in the global tomographic model of Schaeffer and Lebedev (2014). However, in recent 2-plane-wave tomography of Sabah from Greenfield et al., (2022), average lithosphere thickness beneath Sabah is found to be ~100km, with the lithosphere only being thin (<50km) beneath the Semporna Peninsula, consistent with the work of Pilia et al., (2023b) that suggests that the lithosphere here has dripped off.

Until recently, estimates of crustal thickness in Sabah had been limited. Holt (1998) modelled gravity data from Sabah and suggested that the whole of Sabah was underlain by crust >30 km thick, that crustal thicknesses beneath the Crocker Range was ~50 km, and 39 km beneath central Sabah. Estimates of 27±3 km and 33±2 km beneath seismometers KKM and LDM near Kota Kinabalu and Lahad Datu respectively have been made by Lipke (2008) from H-κ stacking of receiver functions. A regional crustal thickness map derived from surface wave data made by Tang and Zheng (2013) estimates crustal thickness beneath Sabah to be 27.5-32.5 km. The deployment of the nBOSS seismic network between 2018-2020 has allowed for more detailed studies of crustal thickness to be conducted. Greenfield et al. (2022) use the 4.1 km/s velocity contour in their shear wave velocity model as a proxy for the Moho and suggest that crustal thicknesses vary from 25-55 km, with the thickest crust beneath the Crocker Range and the Dent Peninsula, and the thinnest crust in north east Sabah. Linang et al. (2022) use Virtual Deep Seismic Sounding (VDSS) to estimate crustal thickness in the range 21 - 46 km, with a similar pattern of thicker and thinner crust.

Until now, due to a lack of seismic instrumentation in the region, it has not been possible to derive a detailed model of the seismic velocity structure of Sabah's crust. Consequently, debates have continued to emerge (e.g., Milsom et al. 2001, Cullen and Burton-Johnson, 2021) about the nature of the crust beneath this part of Borneo and the processes that have shaped it.

In this study, we calculate radial P-wave receiver functions at 70 seismic stations, including the recent nBOSS deployment across Sabah, and jointly invert these with surface wave data to develop the first detailed shear velocity model of the crust in Sabah, as well as map the Moho geometry beneath. These results provide important constraints on processes that have shaped the region.

Data and Methods

Broadband teleseismic data in this study come from two seismic networks deployed in Sabah (Figure 1, Supplementary Table 1). The temporary nBOSS network of 46 seismometers, installed with a ~40x40 km grid spacing, between March 2018 and January 2020, consisted of 18 Güralp 3ESPD instruments and 28 Güralp 6TD instruments (Rawlinson, 2018, Pilia et al., 2019). We also used data from the Malaysian Metrological Service permanent seismic network. In Sabah, this consists of 24 permanently installed Streckeisen STS2/2.5 and SS1-Ranger seismometers, predominantly located in regions of elevated seismicity around Mt Kinabalu and Darvel Bay.

Calculation of radial P receiver functions from 3-component seismograms of teleseismic (30-90° epicentral distance) earthquakes allows us to investigate the structure of the crust, including determining Moho depth and identifying layering within the crust. While useful, the interpretation of receiver functions on their own is inherently non-unique (Ammon et al., 1990), and so Earth structure can be better elucidated when receiver functions are jointly used with other geophysical data, such as surface waves (Özalaybey et al., 1997).

We performed the initial quality control of the seismograms in two stages. First, a total of 27,660 3-component seismograms from March 2018-September 2018 for earthquakes M_w >5 that met the distance criteria were visually inspected. Where the P-wave signal-to-noise ratio was high (e.g., a P arrival could clearly be identified) on all 3 components, these seismograms were classified as 'good' and were taken forward for further analysis. All other seismograms were rejected and classified as 'bad'. Using this classified data set we developed a deep learning algorithm to determine the probability of a 3-component seismogram being suitable for further analysis. The annotated (good or bad) seismograms were converted into spectrograms and 80% of the data were used to train an image classification convolutional neural network, ResNet50, pretrained on ImageNet (He et al., 2016). The data classification algorithm was then tested using the remaining 20 per cent of the data and had a 92.7 per cent accuracy. A total of 57,858 3-component seismograms from

September 2018-January 2020 were then used with the classification algorithm, and only those classified with a greater than 50 per cent probability of being ‘good’ were visually inspected. This significantly reduced the time needed for this stage of data quality control, while resulting in a similar proportion of events being taken forward for further analysis.

After initial quality control, 14,447 seismograms were used to calculate receiver functions using the time-domain iterative deconvolution method of Ligorría and Ammon (1999). Further quality control steps included removal of receiver functions with a poor fit (<70 per cent), and those which appeared noisy, oscillatory or anomalous to other receiver functions from a similar distance and backazimuth on visual inspection. This left a remaining dataset of 3543 receiver functions. Five stations had no usable receiver functions. For stations with usable receiver functions, the number of receiver functions at individual seismometers ranges from 5 at TSM and SGM to 183 at SBA8 (Supplementary Table 1, Supplementary Figure 1). This is due to variations in the amount of data available from individual stations and the noise levels at the installation sites.

Receiver functions at an individual station are stacked together to reduce noise. This stacked receiver function is then used in a joint inversion with surface wave data for shear velocity structure. 1-D fundamental mode Rayleigh wave group velocity dispersion curves were extracted from the GDM52 global compilation (Ekström, 2011) for each station location for a period range 25–250 s. This period range constrains velocities in the lower crust and upper mantle, which helps the inversion overcome the Vp/Vs-depth trade-off inherent to receiver function data.

Dispersion curves and radial P receiver function stacks for each station were inverted for shear velocity structure using joint96 (Herrmann, 2013), an iterative linearized least squares inversion method. Several starting models were tested including constant values of 4.48 km/s, (mantle velocity in the ak135 model - see Kennett et al., 1995), 4.28 km/s, and 3.70 km/s and a Vp/Vs value of 1.79 down to 100 km depth, parameterized into 2 km thick layers, overlying ak135. While there are some small variations in the absolute shear velocities due to differences in the starting models, they are sufficiently small to not alter the interpretation of the structure. We test different relative weights (p value in joint96) of surface waves to receiver function data in the inversion: 0.5, 0.1, 0.05 and 0.01. Models with p=0.5 are smoother than those with a lower p value, reflecting the greater contribution of surface wave data. Overall the models show little variation in structure with p value, indicating that the recovered features are robust (Supplementary Figure 2).

In order to test the stability of the results, the receiver functions at each station were divided into 3 time periods (March 2018-Sept 2018, Sept 2018-March 2019, March 2019-Jan 2020) and were stacked and inverted separately. There was very little difference between the resulting models and those obtained from the complete dataset (Supplementary Figure 3) This gives us further confidence that the results are robust.

Results

Stacked receiver functions

Stacked receiver functions at each station are plotted on cross-sections across Sabah (Figure 2). Cross-section A (Figure 2 (a)) cuts through the highest topography in Sabah in the region around Mt Kinabalu. Heading SE from the NW coast there is a positive arrival that decreases from ~4.5 s to ~3 s delay time at the stations immediately beneath the highest topography. Moving further SE, the delay time of this prominent positive arrival then increases to ~7 s at station SBE4 (dark grey dashed line). At stations to the SE of Mt Kinabalu, this positive arrival is preceded by a large amplitude negative arrival that similarly shows an increase in arrival time from ~3 s at SBF2 to ~5 s at SBE4 (light grey dashed line). There is a clear change in the character of the receiver functions from ~200 km along the cross section, with the portion of cross-section A between SBD5 and SBD7 having a large amplitude positive arrival at ~6-6.5 s (dark grey dashed line).

In cross-section B (Figure 2 (b)), the stations in the Crocker Range have a relatively consistent large amplitude positive arrival (dark grey dashed line) at ~4 s, while at SBB3 and SBD4, immediately to the SE, the largest amplitude positive arrival appears to be at ~6.5 s. Between these stations and those in the vicinity of the Maliau Basin there is a strong positive arrival at ~3.5 s, while at the stations near to the Maliau Basin there is an arrival at ~5 s. At the south-east end of the cross-section, in the Semporna Peninsula, the largest positive arrivals, after the direct P arrival, is again at a shorter delay time of around 4 s.

The peak at ~0 s should correspond to the direct P arrival; however if there are low-velocity sediments in the uppermost crust the P-to-S conversion from the base of these may interfere with the direct P resulting in the first positive arrival being shifted away from 0 s. This is observed at several sites, e.g., SBD6 (Figure 2 (a)) and MALB (Figure 2 (b)) and is anticipated given the thick sedimentary basins (>6 km sediments, Hall, 2013) in Sabah.

Shear velocity structure

Using the 1-D shear wave velocity model beneath each station, 2D composite velocity cross sections have been constructed for several lines across Sabah. The models shown in Figure 3 are derived from the inversions that used p=0.1 and the 3.7 km/s starting model; however, the features remain consistent with the various weightings and starting models tested. The orientations of cross-sections A and B are chosen to be approximately perpendicular to the strike of the Crocker range, while cross-sections C, D, and E are chosen to help further elucidate the 3D crustal structure.

In cross-section A (Figure 3(a)), low velocity sedimentary basins, labelled as 1 in the cross-section, are illuminated offshore to the NW (SBG1) and in the south-eastern half of the cross-section (SE of SBE4), confirming the observation of a broadened, delayed P arrival in the receiver function stacks. Low velocities extend to depths of ~10 km. The most striking feature of this cross-section is a dipping high velocity layer, labelled 2, extending from SBE3 to SBE5 from ~5 km to 50 km depth, with a dip in the cross section to the SE, which overlies a low velocity layer, labelled 3, with a similar dip. This fits the pattern of arrivals seen in the receiver function cross-sections: a seemingly dipping transition from a high velocity to a low velocity layer resulting in a negative arrival, followed by a low to high velocity discontinuity with increasing depth. The velocities observed in the high velocity layer are similar (~4.2 km/s), typically observed in peridotic rocks in the upper mantle. It is noteworthy that rocks of this composition are found in the surface geology in the areas to the east of Mt Kinabalu and around Telupid.

In cross-section B (Figure 3(b)) low velocities, labelled 4, are also observed to ~10 km depth in the vicinity of known sedimentary basins between SBC4 and SBA7. The transition to mantle velocities (~ >4.2 km/s) occurs at ~30-35 km depth in the north-western part of the cross section but deepens to greater than 40 km beneath SBC4. It shallows to ~25 km beneath SBB4 and SBC5, before deepening to ~35 km again beneath the Maliau Basin. This agrees with the pattern of positive arrivals observed in the stacked receiver functions, with those for stations between the Crocker Range and the Maliau Basin experiencing the shortest delay times. At the southeast end of cross-section B, the crust beneath SBA8 and SBA9 has lower velocities (~3.9 km/s) at the gradient interpreted to be the Moho, labelled 5, than beneath stations elsewhere in the section.

The differences in crustal structure from south to north through western Sabah is highlighted in cross-section C (Figure 3(c)). The crustal structure at the north-east end of this section, to the north of Mt Kinabalu, has a different character to that in the central portion of the section (between SBD2 and SBE3). In the north east, very high velocities (>4.2 km/s), labelled 6, are observed at ~20 km, while in the central portion they are generally low (<3.4 km/s) at this depth in a somewhat discontinuous layer, labelled 7, likely the dipping low velocity layer observed in cross-section A. Cross-section D (Figure 3(d)) cuts to the east of the Crocker Range, through the Maliau Basin. In the south west of this section there is a northeasterly dipping transition from crust to mantle velocities (~4.2 km/s) from 25 to 45 km depth between SBA3 and the Maliau Basin. At SBC5 it decreases sharply to a depth of 25 km, the depth it is also observed to be at between SBE4 and SBF4. Beneath SBD4 relatively high velocities are observed in the upper crust, labelled 8, and low velocities are observed between 25 and 45km depth. This location corresponds with where ophitic material is found on the surface around Telupid (e.g. Hall 2013) . In the south of cross-section E (Figure 3(e)), which cuts through the Semporna and Dent Peninsulas, the transition between crustal and mantle velocities at ~35 km depth is relatively gradual. This contrasts with further north, where this transition is sharper, and upper mantle velocities are faster.

Moho depth

The depth of the Moho beneath each station is picked from its corresponding 1-D shear velocity model at the depth that corresponds to the base of the steepest positive velocity gradient where shear velocity exceeds 4 km/s

(Figure 4). The depth of the Moho is found to vary from 22 km at TLM to 60 km at MTM, although most other measurements are <48 km. The deepest Moho is found in a SW-NE trending band on the eastern edge of the Crocker Range, where the Moho depth exceeds 40 km. It is also relatively deep (40-44 km) beneath the Maliau Basin and beneath other circular basins to the north of the Maliau Basin, and to the west of the Segama ophiolite. The shallowest Moho depth (22-26 km) is found in a band between the Crocker Range and the circular basins, with changes in Moho depth of ~15-25 km occurring over short lateral distances (~20 km).

At the stations marked with white hexagons in Figure 4, it was not clear where the Moho should be picked. For instance, at a subset of stations (e.g., SBD6, SBD7, and SBC8) there is a very gradual increase in velocities over a wide (~40 km) depth range (Supplementary Figure 4), while at other stations (e.g., SBD5, SBE4, and SBG3) the models have two steep velocity gradients, both of which could represent plausible Moho locations given those found elsewhere in Sabah, for example at 28km and 58km for SBD5

Discussion

Processes affecting crustal thickness

It is important to account for the effect of the interference between conversions and multiples (e.g., Gilligan et al., 2014): a consequence is that the largest signal on a receiver function should not necessarily be interpreted as being due to the velocity increase at the Moho. However, there is a consistent pattern between the positive arrivals observed in the stacked receiver functions and the velocity changes at the Moho observed in the models from joint inversion, suggesting that the receiver functions can, in this instance, provide an interpretable picture for trends in Moho depth.

The variations in crustal thickness across Sabah observed in this study are in general agreement with the estimates made by recent studies using 2-plane-wave tomography (Greenfield et al., 2022) and virtual deep seismic sounding (Linang et al., 2022): central Sabah appears to have significantly thinner crust than that beneath the Crocker Range and the Circular Basins (Supplementary Figure 5). One notable difference with the Greenfield et al., (2022) Moho estimate is beneath the Semporna Peninsular they observe thick crust (>55km), while in this study we observe crustal thickness of ~34km. This difference is likely to arise due to Greenfield et al., (2022) using the 4.1km/s shear velocity contour as a proxy for Moho depth, and this, as discussed below, may not be an appropriate velocity proxy for the lower crust/upper mantle beneath the Semporna Peninsular.

The pattern of thicker and thinner crust broadly agrees with the estimates of Holt (1998) using gravity data; however, between the Crocker Range and thickened crust beneath the circular basins we observe a significantly thinner crust (e.g., 25 and 24 km at SBC5 and SBC6 respectively) than the 32 km suggested by Holt (1998). Modelling gravity data is notoriously non-unique, and Holt (1998) uses a very simple model for crustal densities. Given the lack of other constraints on the properties of the crust at the time this may have been appropriate; however the lateral and vertical heterogeneity of the crust demonstrated in this study indicates a more complex model is required, which may alter the estimates of crustal thickness from the gravity data.

It should be noted that the crust in this study is thicker throughout much of Sabah than was shown in interpretative cross-section of Hall (2013), which bases Moho depth off the results of Holt (1998), modified for denser material. Hall (2013)'s cross-section shows a maximum Moho depth of 40km beneath the Crocker Range, and around 20km beneath both the circular basins and the Dent and Semporna peninsulas. Further, our estimates of crustal thickness shows a significantly different pattern and depths to the estimates made by Tang and Zheng (2013). They report crustal thicknesses of ~27.5 to 32.5km, increasing southward across Sabah, based on the depth of the 4 km/s velocity contour in their shear velocity model. This model encompasses the whole of the South China Sea and surrounding region and, as such, has more limited resolution in Sabah compared to this study and others (Greenfield et al., 2022, Linang et al., 2022) that have used the data from the nBOSS network. The thicker crust we observe, compared to earlier estimates, may mean that there is a larger contribution from regional tectonic shortening to the regional uplift observed by Roberts et al., (2018).

The relatively thick crust (>40 km) beneath the Crocker Range, particularly on the eastern side, is likely to have been thickened during the Sabah Orogeny (~23 Ma), when the Dangerous Grounds block collided with the western edge of northern Borneo at the final stage of the subduction of the proto-South

China Sea (e.g. Hutchison et al., 2000, Hall 2013, Rangin et al., 1999). The velocity discontinuity picked as the Moho for many stations in the Crocker Range is the base of the SE dipping slow velocities seen in cross-section A, which we interpret as the base of the underthrust Dangerous Grounds crust.

Extension, related to the roll-back of the Celebes Sea slab (e.g., Hall, 2013), could have thinned the crust in central Sabah to 20-25 km. Indeed, Tsikouras et al. (2021) argue that the basalts they date to 9-10 Ma in the Telupid area, are rift-related, thus implying significant extension and crustal thinning, although this is disputed by Cullen and Burton-Johnson (2021). A double discontinuity is observed in our study in the 1D velocity models at some stations (e.g., SBE4), and could indicate that it may not necessarily be appropriate to simply interpret the velocity gradient at ~20-25 km as a single Moho. If the crust is 20-25 km thick, the question as to the extent to which this crust may have been thinned remains, i.e., what was the pre-extensional crustal thickness? Greenfield et al. (2022) assume that it was 40-50 km, as is observed beneath the Crocker Range and circular basins, and thus calculate a stretching factor of 1.3-2. However, if this area was not significantly thickened during the Sabah Orogeny, which is plausible given the lack of underthrust Dangerous Grounds material observed in this study, then pre-extensional thickness may have been less to begin with.

Related to the question of pre-extensional thickness is whether the ~45 km thick crust observed beneath the Maliau Basin and other circular basins is a result of thickening during the Sabah orogeny (~23 Ma). After thickening it may have been been separated from other thickened crust beneath the

Crocker Range as a result of extension (e.g., in a crustal scale boudinage process as suggested by Linang et al. (2022)). Alternatively, the crust may have been thickened at a later point in time. Tongkul and Chang (2003) suggest that eastern Sabah experienced N-S compression in the mid Middle Miocene (~13 Ma), which led to the segmentation of the large basin in eastern Sabah that had been active in the Early Miocene, and NW-SE compression in the late Upper Miocene (~7-5 Ma), which enhanced the circular shape of the basins, with a period of sediment deposition in between these two compressional events. It may be that during these compressional episodes, potentially associated with Celebes Sea subduction, some crustal thickening occurred beneath the circular basins.

While areas of the highest topography may be anticipated to have some of the thickest crust, intriguingly beneath the stations in the vicinity of the 4095m high Mt Kinabalu the crust is only 30-35km thick. The Kinabalu Granite was emplaced between 7.2-7.8Ma (Cottam et al., 2013), well after the termination proto-South China Sea subduction, thus it would be expected that the crust in this region would have been thickened as a result of this collision. The thermomechanical modelling of Pilia et al., (2023b) shows that as a result of a downwelling drip, e.g the Semporna drip, a region of initially thick crust can be thinned. This thinning could facilitate melting of the lower crust, thus it may be that both the presence of the Kinabalu pluton and the thinner-than-anticipated crust we observe can both be explained by part of the lithosphere having dripped off beneath the Semporna peninsula.

Crustal structure

Given the diversity of the surface geology in Sabah, it is unsurprising that that the crust shows considerable variation. The key elements of our interpretation are shown in Figure 5.

We interpret the low velocity (<3.4 km/s) layer seen dipping to the south east from the west coast of Sabah to the eastern edge of the Crocker Range in Cross-section A (Figure 3(a)) as Dangerous Grounds material that has been underthrust beneath Sabah. Underthrusting of attenuated Dangerous Grounds crust has been proposed as the mechanism by which subduction of the proto-SCS stopped (e.g., Hall, 2013, Morley and Back, 2008, Hutchison, 2000), but this is arguably the first time it has been imaged. Cross-section B (Figure 3(b)), which cuts to the south of Cross-section A, also has a low velocity layer at depths of 20-25 km. In this instance this layer does not seem to dip. We consider this to also be underthrust Dangerous Grounds crust, although this suggests potential along strike variation in the nature of the collision between Sabah and the Dangerous Grounds. Rangin et al. (1999), considering the whole of the proto-SCS, argue that the proto-SCS basin was narrower off the coast of Borneo than the Sulu Sea, and it may be that the differences we observe in underthrust Dangerous Grounds crust are a manifestation of this. Furthermore, Greenfield et al., (2022) note that the lithosphere is thinner in the southwest of Sabah, again suggesting that different processes may have influenced this area compared to those further north.

Overlying the low velocity layer in Cross-section A is a high velocity layer, also dipping to the south east, with velocities exceeding 4 km/s in what has been interpreted as the upper to mid crust. The velocities are consistent with this being mafic to ultramafic material, and it appears to lie beneath areas of peridotic rocks near Ranau and ophitic rocks near Telupid. We therefore interpret this as obducted ophitic material, although it is not possible to constrain the timing of the emplacement from this study, e.g., it may be the result of late Mesozoic rifting (Tsikouras et al., 2021), or it could have been emplaced earlier (e.g., Cullen and Burton-Johnson 2021).

The crustal structure of the northern tip of Sabah (to the north of SBF2) is distinct from areas to the south, as is particularly seen in Cross-section C (Figure 3(c)), suggesting that distinct geological processes have shaped this region. The change in the character of the crustal structure is in the same place where there is a change in strike of the surface geology, from ~SW-NE to the south to ~WNW-ESE in the north (Tongkul 1990), in the vicinity of Mt Kinabalu. Moreover, it is approximately coincident with where the fast velocity anomaly in the upper mantle that Pilia et al. (2023a) associate with the proto-South China Sea slab terminates. Tongkul (1994) suggests, based on the relationships between sedimentary rocks in this region, that the basement here - Mesozoic oceanic crust - is uplifted relative to the area to the south. Tongkul (1994) further suggests that this region was affected by the collision with the Reed Bank, resulting in N-S compression, while further south the collision was with the Dangerous Grounds block. Gozzard et al., (2018) observe that the crust beneath the Reed Bank has not been thinned in the same way as the Dangerous Grounds block. Franke et al., (2008) also note the presence of the Kudat block off the eastern shore of northernmost Sabah, which active source seismic data suggests has a different crustal structure. It may be that the different properties of blocks colliding with Sabah, as well as the orientation of the collisions, resulted in the contrasting crustal structure we observe today: underthrust material to the south but not at the northern tip of Sabah.

In the east of Sabah, the lower crust and upper mantle beneath stations in the Semporna Peninsula (SBA8 and SBA9) is relatively slow (~3.8-4 km/s for the uppermost mantle compared to 4.3-4.5 km/s elsewhere). This is similar to the results from the two-plane wave tomography of Greenfield et al. (2022). Volcanism in this area occurred until at least 0.2 Ma (Lai et al., 2021) and potentially as recently as 24-27 ka (Kirk, 1968; Bellwood, 1988; cited in Tjia et al., 1992) with hot springs found in the vicinity of Tawau today, with water temperatures of up to 75°C (Siong et al., 1991). Pilia et al. (2023b) and Greenfield et al. (2022) propose that part of the lithosphere has been removed beneath the Semporna Penisula and has been replaced by hot asthenospheric material. This would mean that the remaining crust and mantle would be expected to be warm and thus seismically slow, as we observe here.

Conclusion

We present a high-resolution crustal shear velocity model of Sabah, northern Borneo, from the joint inversion of P receiver functions and surface wave data. We image, for the first time, Dangerous Grounds crust underthrust beneath most of the Crocker Range. This has had the effect of thickening the crust beneath the present-day mountain range, with crustal thicknesses exceeding 40 km. However, beneath Mt Kinabalu, crustal thicknesses are only in the range 30-35km, supporting earlier ideas (Cottam et al., 2013, Sapin et al., 2013, Tsikouras et al., 2021, Pilia et al., 2023b) that some degree of crustal thinning may have been involved in its emplacement. Thinner crust (~25 km) between the Crocker Range and the Circular Basins may be due to extension related to the rollback of the Celebes Sea slab (Hall, 2013), although the amount of extension remains unclear given that pre-extensional crustal thickness remains unknown. Thicker crust (>40 km) beneath the Maliau and other circular basins suggests that these areas have experienced some degree of crustal thickening, which given the late-mid Miocene age of the sediments that have been deformed is likely to have occurred later than the ~21 Ma Sabah Orogeny. Relatively slow velocities in the lower crust and upper mantle beneath the Semporna Peninsula support work by Pilia et al. (2023b) and Greenfield et al. (2021) that lithospheric delamination has occurred here.

Overall, we observe a high degree of heterogeneity in the crustal structure beneath Sabah, on length scales of 10s of kilometres. This highlights the complexity of subduction, collisional, post-subduction, and extensional processes that have shaped Sabah over the Cenezoic, and reinforces the importance of dense instrumentation in order to better understand tectonic activity that has occurred in similar settings.

Acknowledgements

Thanks to all those who were involved in the deployment, servicing and recovery of the nBOSS network between March 2018 and January 2020. Many thanks to the landowners throughout Sabah who hosted seismometers. Seismometers used in the nBOSS network were provided by the University of Cambridge, the University of Aberdeen (Aberdeen University Geophysical Equipment Repository – AUGER), and the Natural Environment Research Council (NERC) Geophysical Equipment Facility though SeisUK (loan 1038). We thank MetMalaysia for providing access to their restricted continuous waveform data recorded by their permanent MY network in Sabah. A.G was supported by a Royal Astronomical Society Independent Research Fellowship. S. P was supported by the Natural Environmental Research Council (NERC) Grant NE/R013500/1 and from the European Union's Horizon 2020 Research and Innovation Program under Marie Skłodowska-Curie Grant Agreement 790203. T.G. was supported by an Early Career Fellowship from the Leverhulme Trust. We have made of several open source Python packages in our analysis and visualisation, including Matplotlib (Hunter, 2007); and ObsPy (Beyreuther et al., 2010). A number of figures were produced using the Generic Mapping Tools version 6 (Wessel et al., 2019). We thank Robert Herrmann for making the Computer Programs in Seismology freely available.

Data availability

Part of the nBOSS dataset is accessible through the IRIS Data Management service (https://www.fdsn.org/networks/detail/YC_2018/). Data from the remaining nBOSS stations will be available from February 2024. Data from the Malaysian national seismic network (https://www.fdsn.org/networks/detail/MY/) are restricted but may be obtained by contacting the Malaysian Meteorological Department. The exceptions to this are stations KKM and LDM which are also available through the IRIS Data Management service.

Author contributions

A.G.: Formal analysis, conceptualisation, funding acquisition, investigation, resources, visualisation, writing – original draft; **D.C.:** Investigation, resources, writing - review and editing; **N.R.:** Conceptualisation, funding acquisition, resources, investigation, writing – review and editing; **F.T.:** Conceptualisation, resources, investigation; **S.P.:** Investigation, writing – review and editing, funding acquisition; **T.G.:** Investigation, writing – review and editing; **C.B.:** Data curation, investigation.

References

Amaru, M. L. (2007). *Global travel time tomography with 3-D reference models* (Vol. 274). Utrecht University.

Ammon, C. J., Randall, G. E., & Zandt, G. (1990). On the nonuniqueness of receiver function inversions. *Journal of Geophysical Research: Solid Earth*, *95*(B10), 15303-15318.

Bacon, C. A., Rawlinson, N., Pilia, S., Gilligan, A., Wehner, D., Cornwell, D. G., & Tongkul, F. (2022). The Signature of Lithospheric Anisotropy at Post-Subduction Continental Margins: New Insight From XKS Splitting Analysis in Northern Borneo. *Geochemistry, Geophysics, Geosystems*, *23*(11), e2022GC010564.

Balaguru, A., & Nichols, G. (2004). Tertiary stratigraphy and basin evolution, southern Sabah (Malaysian Borneo). *Journal of Asian Earth Sciences*, *23*(4), 537-554.

Barckhausen, U., Engels, M., Franke, D., Ladage, S., & Pubellier, M. (2014). Evolution of the South China Sea: Revised ages for breakup and seafloor spreading. *Marine and Petroleum Geology*, *58*, 599-611.

Bellwood, P. S. (1988). Archaelogical research in south-eastern Sabah. Sabah Museum and State Archives

Beyreuther, M., Barsch, R., Krischer, L., Megies, T., Behr, Y., & Wassermann, J. (2010). ObsPy: A Python toolbox for seismology. *Seismological Research Letters*, *81*(3), 530-533.

Burton-Johnson, A., Macpherson, C. G., Muraszko, J. R., Harrison, R. J., & Jordan, T. A. (2019). Tectonic strain recorded by magnetic fabrics (AMS) in plutons, including Mt Kinabalu, Borneo: A tool to explore past tectonic regimes and syn-magmatic deformation. *Journal of Structural Geology*, *119*, 50-60.

Burton-Johnson, A., Macpherson, C. G., Millar, I. L., Whitehouse, M. J., Ottley, C. J., & Nowell, G. M. (2020). A Triassic to Jurassic arc in north Borneo: Geochronology, geochemistry, and genesis of the Segama Valley Felsic Intrusions and the Sabah ophiolite. *Gondwana Research*, *84*, 229-244.

Burton-Johnson, A., & Cullen, A. B. (2023). Continental rifting in the South China Sea through extension and high heat flow: An extended history. *Gondwana Research*, 120, 235-263

Cottam, M. A., Hall, R., Sperber, C., Kohn, B. P., Forster, M. A., & Batt, G. E. (2013). Neogene rock uplift and erosion in northern Borneo: evidence from the Kinabalu granite, Mount Kinabalu. *Journal of the Geological Society*, *170*(5), 805-816.

Cullen, A., & Burton-Johnson, A. (2021). [Comment] New zircon radiometric U-Pb ages and Lu-Hf isotopic data from the ultramafic-mafic sequences of Ranau and Telupid (Sabah, eastern Malaysia): Time to reconsider the geological evolution of Southeast Asia?. *Geology*, *49*(11), 541-541.

Forsyth, D., & Uyeda, S. (1975). On the relative importance of the driving forces of plate motion. *Geophysical Journal International*, *43*(1), 163-200.

Franke, D., Barckhausen, U., Heyde, I., Tingay, M., & Ramli, N. (2008). Seismic images of a collision zone offshore NW Sabah/Borneo. *Marine and Petroleum Geology*, *25*(7), 606-624.

Ekström, G. (2011). A global model of Love and Rayleigh surface wave dispersion and anisotropy, 25-250 s. *Geophysical Journal International*, *187*(3), 1668-1686.

Foley, S., Tiepolo, M., & Vannucci, R. (2002). Growth of early continental crust controlled by melting of amphibolite in subduction zones. *Nature*, *417*(6891), 837-840.

Franke, D. (2013). Rifting, lithosphere breakup and volcanism: Comparison of magma-poor and volcanic rifted margins. *Marine and Petroleum geology*, *43*, 63-87.

Gilligan, A., Roecker, S. W., Priestley, K. F., & Nunn, C. (2014). Shear velocity model for the Kyrgyz Tien Shan from joint inversion of receiver function and surface wave data. *Geophysical Journal International*, *199*(1), 480-498.

Gozzard, S., Kusznir, N., Franke, D., Cullen, A., Reemst, P., & Henstra, G. (2019). South China Sea crustal thickness and oceanic lithosphere distribution from satellite gravity inversion. *Petroleum Geoscience*, *25*(1), 112-128.

Greenfield, T., Gilligan, A., Pilia, S., Cornwell, D. G., Tongkul, F., Widiyantoro, S., & Rawlinson, N. (2022). Post‐Subduction Tectonics of Sabah, Northern Borneo, Inferred From Surface Wave Tomography. *Geophysical Research Letters*, *49*(3), e2021GL096117.

Hall, R. (2013). Contraction and extension in northern Borneo driven by subduction rollback. *Journal of Asian Earth Sciences*, *76*, 399-411.

Hall, R., & Spakman, W. (2015). Mantle structure and tectonic history of SE Asia. *Tectonophysics*, *658*, 14-45.

He, K., Zhang, X., Ren, S., & Sun, J. (2016). Deep residual learning for image recognition. In *Proceedings of the IEEE conference on computer vision and pattern recognition* (pp. 770-778).

Herrmann, R. B. (2013). Computer programs in seismology: An evolving tool for instruction and research. *Seismological Research Letters*, *84*(6), 1081-1088.

Hunter, J. D. (2007). Matplotlib: A 2D graphics environment. *Computing in science & engineering*, *9*(03), 90-95.

Hutchison, C. S., Bergman, S. C., Swauger, D. A., & Graves, J. E. (2000). A Miocene collisional belt in north Borneo: uplift mechanism and isostatic adjustment quantified by thermochronology. *Journal of the Geological Society*, *157*(4), 783-793.

Holt, R. A. (1998). *The gravity field of Sundaland-acquisition, assessment and interpretation*. University of London, University College London (United Kingdom)

Huang, Z., Gradstein, F.M., and Louden, K.E., (1991). Subsidence and sedimentation analysis of marginal basins: Celebes Sea and Sulu Sea, Leg 124, Sites 767 and 768, in Silver, E.A., Rangin, C., von Braymann, M.T., et al, Proceedings of the Ocean Drilling Program, *Scientific Results* , 124, 399-407

Johnston, F. K., Turchyn, A. V., & Edmonds, M. (2011). Decarbonation efficiency in subduction zones: Implications for warm Cretaceous climates. *Earth and Planetary Science Letters*, *303*(1-2), 143-152.

Kennett, B. L., Engdahl, E. R., & Buland, R. (1995). Constraints on seismic velocities in the Earth from traveltimes. *Geophysical Journal International*, *122*(1), 108-124.

Kirk, H. J. C. (1968). The igneous rocks of the Sarawak and Sabah. *Geological Survey Borneo Region, Malaysia, Bull*, *5*, 201.

Lai, C. K., Xia, X. P., Hall, R., Meffre, S., Tsikouras, B., Rosana Balangue‐Tarriela, M. I., ... & Norazme, N. A. (2021). Cenozoic Evolution of the Sulu Sea Arc‐Basin System: An Overview. *Tectonics*, *40*(2), e2020TC006630.

Levander, A., Schmandt, B., Miller, M. S., Liu, K., Karlstrom, K. E., Crow, R. S., Lee, C.-T. A., & Humphreys, E. D. (2011). Continuing Colorado plateau uplift by delamination-style convective lithospheric downwelling. *Nature*, *472*(7344), 461-465.

Li, C. F., Xu, X., Lin, J., Sun, Z., Zhu, J., Yao, Y., ... & Zhang, G. L. (2014). Ages and magnetic structures of the South China Sea constrained by deep tow magnetic surveys and IODP Expedition 349. *Geochemistry, Geophysics, Geosystems*, *15*(12), 4958-4983.

Li, Z. H., Liu, M., & Gerya, T. (2016). Lithosphere delamination in continental collisional orogens: A systematic numerical study. *Journal of Geophysical Research: Solid Earth*, *121*(7), 5186-5211.

Ligorría, J. P., & Ammon, C. J. (1999). Iterative deconvolution and receiver-function estimation. *Bulletin of the seismological Society of America*, *89*(5), 1395-1400.

Linang, H. T., Pilia, S., Rawlinson, N., Bacon, C. A., Gilligan, A., Cornwell, D. G., & Tongkul, F. (2022). Collision-induced subduction polarity reversal explains the crustal structure of northern Borneo: New results from Virtual Deep Seismic Sounding (VDSS). *Geophysical Research Letters*, *49*(19), e2022GL099123.

Lipke, K. (2008). Seismologic investigation of the Sunda arc region with receiver functions. *Potsdam: University of Potsdam*.

Macpherson, C. G., Chiang, K. K., Hall, R., Nowell, G. M., Castillo, P. R., & Thirlwall, M. F. (2010). Plio-Pleistocene intra-plate magmatism from the southern Sulu Arc, Semporna peninsula, Sabah, Borneo: Implications for high-Nb basalt in subduction zones. *Journal of Volcanology and Geothermal Research*, *190*(1-2), 25-38.

Milsom, J., Holt, R., Hutchison, C. S., Bergman, S. C., Swauger, D. A., & Graves, J. E. (2001). Discussion of a Miocene collisional belt in north Borneo: uplift mechanism and isostatic adjustment quantified by thermochronology: Journal, Vol. 157, 2000, 783–793. *Journal of the Geological Society*, *158*(2), 396-400.

Morley, C. K., & Back, S. (2008). Estimating hinterland exhumation from late orogenic basin volume, NW Borneo. *Journal of the Geological Society*, *165*(1), 353-366.

Özalaybey, S., Savage, M. K., Sheehan, A. F., Louie, J. N., & Brune, J. N. (1997). Shear-wave velocity structure in the northern Basin and Range province from the combined analysis of receiver functions and surface waves. *Bulletin of the Seismological Society of America*, *87*(1), 183-199.

Pilia, S., Rawlinson, N., Gilligan, A., & Tongkul, F. (2019). Deciphering the fate of plunging tectonic plates in Borneo. *Eos, Transactions American Geophysical Union*, *100*(10), 18-23.

Pilia, S., Rawlinson, N., Hall, R., Cornwell, D. G., Gilligan, A., & Tongkul, F. (2023a). Seismic signature of subduction termination from teleseismic P-and S-wave arrival-time tomography: The case of northern Borneo. *Gondwana Research*, *115*, 57-70.

Pilia, S., Davies, D. R., Hall, R., Bacon, C. A., Gilligan, A., Greenfield, T., Tongkul, F., Kramer, S. C., Wilson, C. R., Ghelichkhan, S., Cornwell, D. G., Colli, L., & Rawlinson, N. (2023b). Post-subduction tectonics induced by extension from a lithospheric drip. *Nature Geoscience*, 1-7.Rangin, C., Spakman, W., Pubellier, M., & Bijwaard, H. (1999). Tomographic and geological constraints on subduction along the eastern Sundaland continental margin (South-East Asia). *Bulletin de la Société géologique de France*, *170*(6), 775-788.

Rawlinson, N. (2018). *Northern Borneo Orogeny Seismic Survey* [Data set]. International Federation of Digital Seismograph Networks. https://doi.org/10.7914/SN/YC_2018

Roberts, G. G., White, N., Hoggard, M. J., Ball, P. W., & Meenan, C. (2018). A Neogene history of mantle convective support beneath Borneo. *Earth and Planetary Science Letters*, *496*, 142-158.

Sapin, F., Hermawan, I., Pubellier, M., Vigny, C., & Ringenbach, J. C. (2013). The recent convergence on the NW Borneo Wedge—a crustal-scale gravity gliding evidenced from GPS. *Geophysical Journal International*, *193*(2), 549-556.

Schaeffer, A. J., & Lebedev, S. (2013). Global shear speed structure of the upper mantle and transition zone. *Geophysical Journal International*, *194*(1), 417-449.

Siong, L. P., Intang, F., & On, C. F. (1991). Geothermal prospecting in the Semporna Peninsula with emphasis on the Tawau area. *Geological Society of Malaysia, Bulletin 29*, 135-155

Takashima I., Nazri, A. A., Lim, P. S., Koseki, T., Mouri, Y., Nasution, A., & Sucipta, I. E., (2004). Thermoluminescence age determination of quaternary volcanic rocks and alteration products at Tawau area, Sabah, Malaysia. *Journal of the Geothermal Research Society of Japan*, *26*(3), 273-283.

Tang, Q., & Zheng, C. (2013). Crust and upper mantle structure and its tectonic implications in the South China Sea and adjacent regions. *Journal of Asian Earth Sciences*, *62*, 510-525.
Tjia, H. D., Komoo, I., Ali, C. A., & Tahir, S. H. (1992). Geology of Taman Bukit Tawau, Semporna Peninsula, Sabah. *Geological Society of Malaysia, Bulletin 31*, 113-131

Tongkul, F. (1990). Structural style and tectonics of Western and Northern Sabah. *Geological Society of Malaysia, Bulletin 27*, 227-239

Tongkul, F. (1991). Tectonic evolution of Sabah, Malaysia. *Journal of Southeast Asian Earth Sciences*, *6*(3-4), 395-405.

Tongkul, F. (1994). The geology of Northern Sabah, Malaysia: its relationship to the opening of the South China Sea Basin. *Tectonophysics*, *235*(1-2), 131-147.

Tongkul, F., and Chang, F. K. (2003) Structural geology of the Neogene Maliau Basin, Sabah. *Geological Society of Malaysia, Bulletin 47*, 51-61

Tsikouras, B., Lai, C. K., Ifandi, E., Teo, C. H., & Xia, X. P. (2021). New zircon radiometric U-Pb ages and Lu-Hf isotopic data from the ultramafic-mafic sequences of Ranau and Telupid (Sabah, eastern Malaysia): Time to reconsider the geological evolution of Southeast Asia?. *Geology*, *49*(7), 789-793.

Wehner, D., Blom, N., Rawlinson, N., Böhm, C., Miller, M. S., Supendi, P., & Widiyantoro, S. (2022). SASSY21: A 3-D Seismic Structural Model of the Lithosphere and Underlying Mantle Beneath Southeast Asia From Multi-Scale Adjoint Waveform Tomography. *Journal of Geophysical Research: Solid Earth*, *127*(3), e2021JB022930.

Wessel, P., Luis, J. F., Uieda, L., Scharroo, R., Wobbe, F., Smith, W. H., & Tian, D. (2019). The generic mapping tools version 6. *Geochemistry, Geophysics, Geosystems*, *20*(11), 5556-5564.

Zandt, G., Gilbert, H., Owens, T. J., Ducea, M., Saleeby, J., & Jones, C. H. (2004). Active foundering of a continental arc root beneath the southern Sierra Nevada in California. *Nature*, *431*(7004), 41-46.

Zenonos, A., De Siena, L., Widiyantoro, S., & Rawlinson, N. (2019). P and S wave travel time tomography of the SE Asia-Australia collision zone. *Physics of the Earth and Planetary Interiors*, *293*, 106267.

Figures

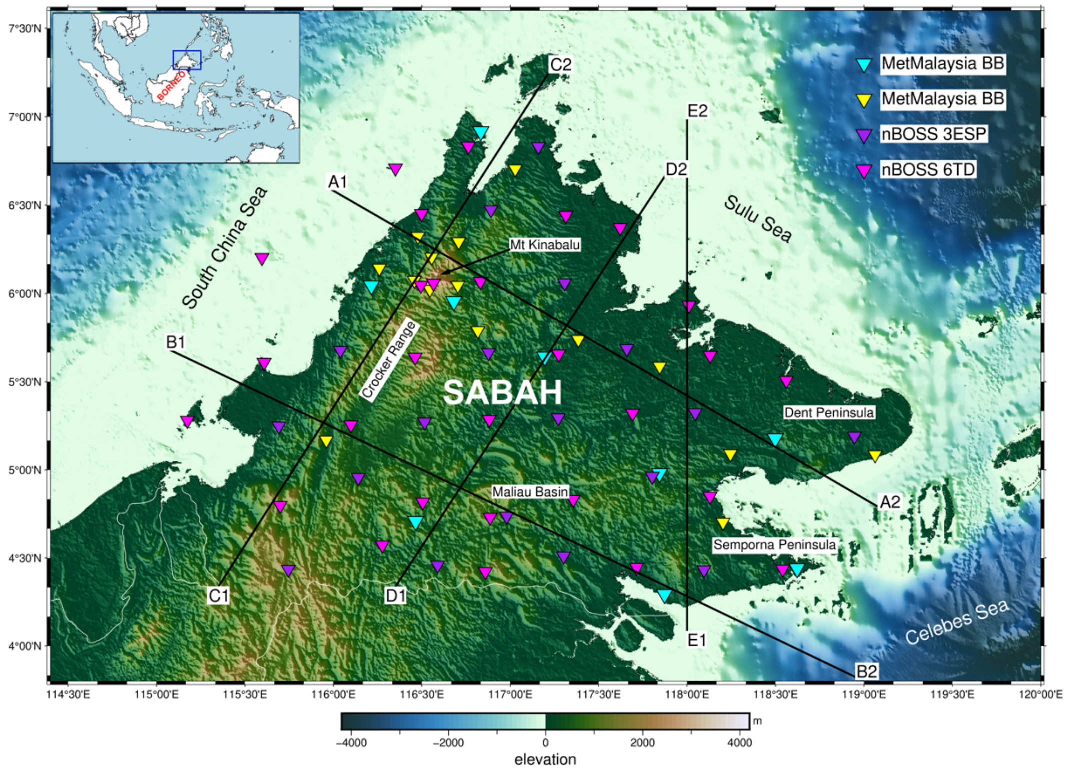

Figure 1: Map of seismometer stations in Sabah used in this study. Blue triangles are MetMalaysia seismometers deployed before 2017, yellow triangles are MetMalaysia seismometers deployed after 2017. Pink (6TD) and Purple (3ESP) triangles are seismometers deployed as part of the nBOSS project. Lines of section are shown: A1-A2 (6.56°N 115.97°E 4.78°N 119.09°E), B1-B2 (5.691°N 115.05°E - 3.82°N 118.96°E), C1-C2 (4.25°N 115.30°E - 7.26°N 117.23°E), D1-D2(4.25°N 116.30°E - 6.67°N 117.88°E) E1-E2 (4°N 118°E - 4°N 7°E)

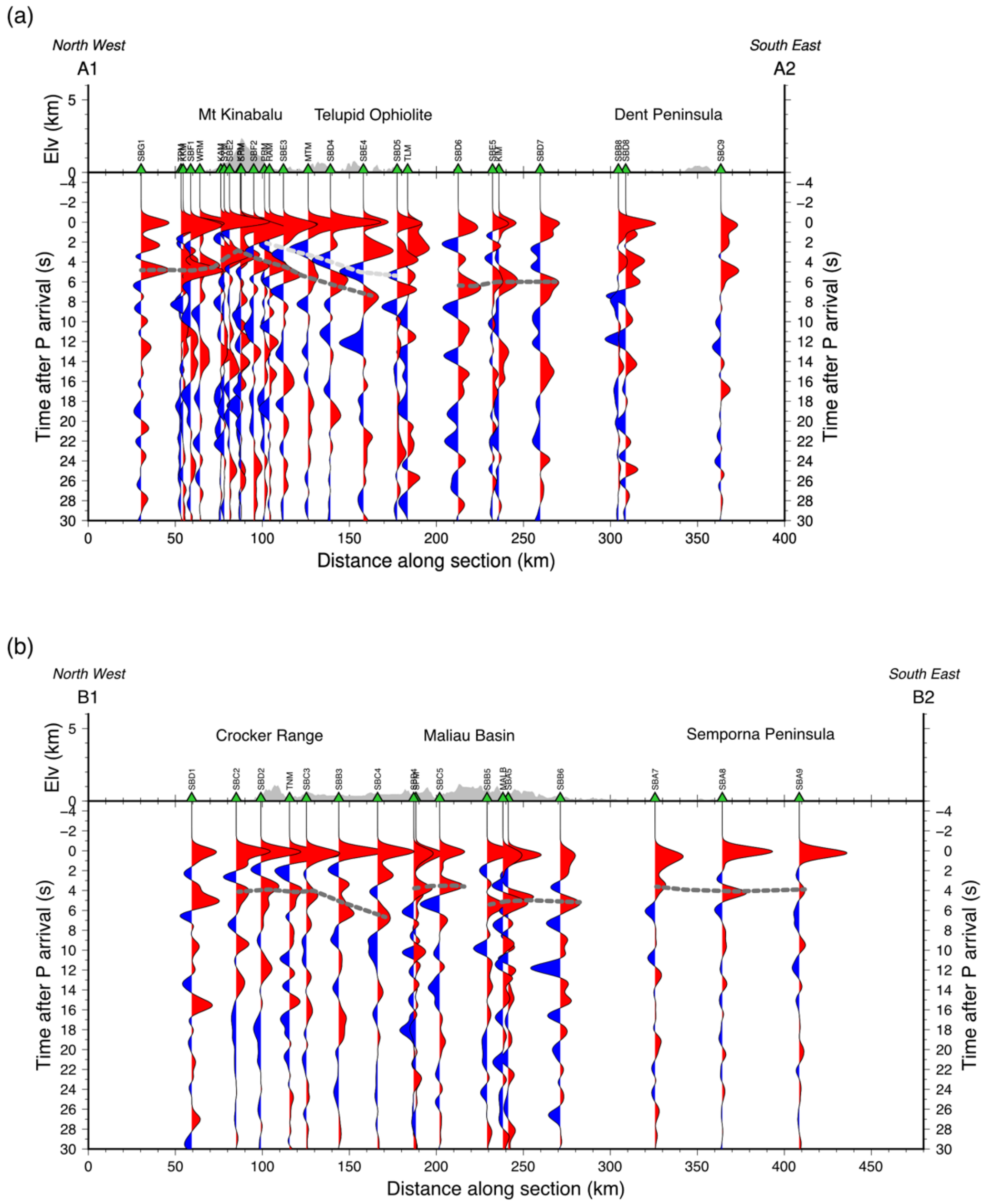

Figure 2: Stacked receiver functions along the lines (a) A1-A2 and (b) B1-B2. Positive arrivals are filled red, and negative arrivals are filled blue. In both cases receiver functions from stations within 50 km of each line have been projected onto the section, along with their respective station (green triangles), and topography is plotted above. The dark grey dashed line highlights positive arrivals, likely from the P-to-S conversion at the Moho. The

light grey dashed line highlights negative arrivals corresponding to a velocity increase with depth in the crust.

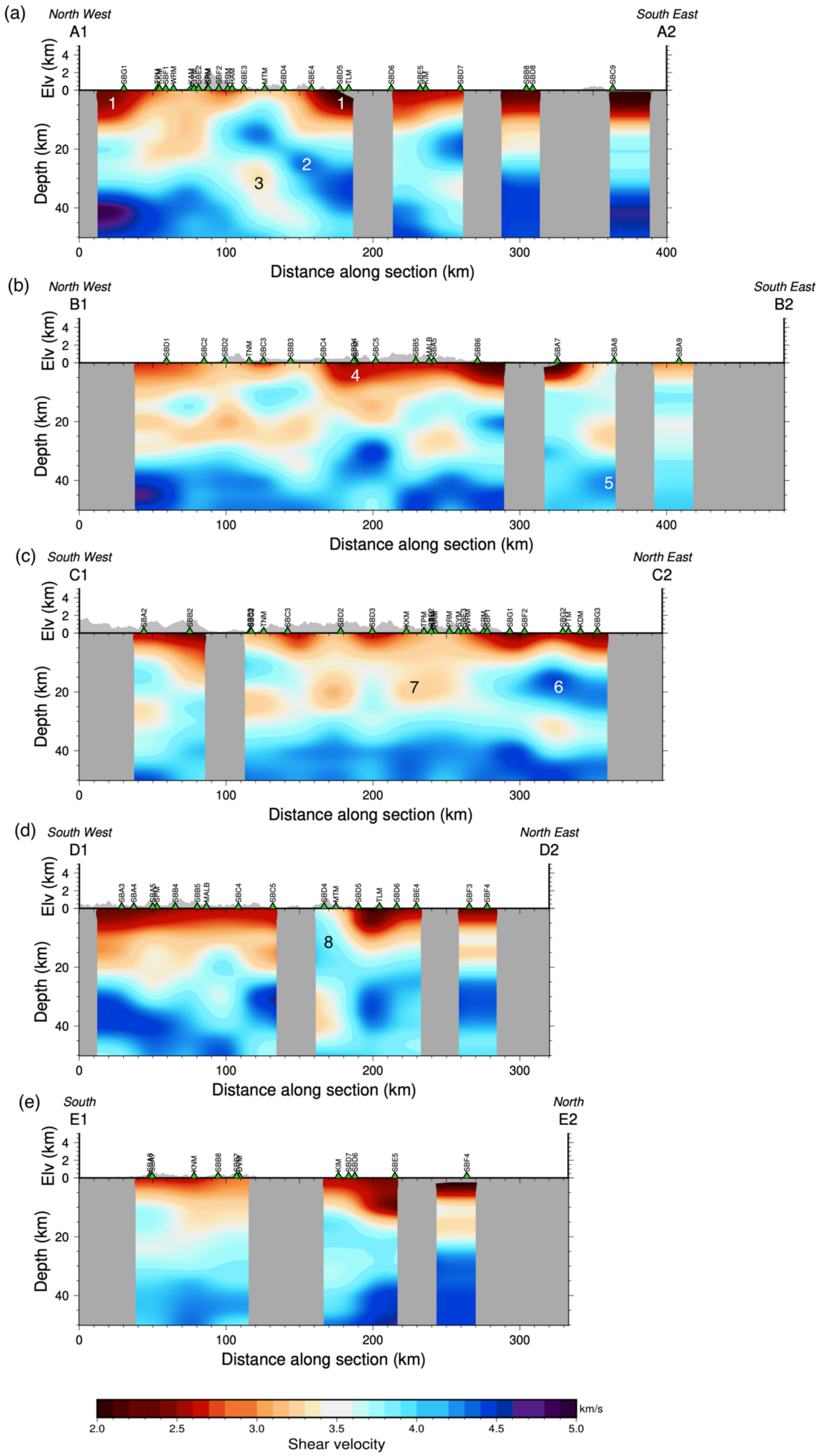

(a)
North West
South East
A1
A2
Elv (km)
Depth (km)
Distance along section (km)
(b)
North West
South East
B1
B2
(c)
South West
North East
C1
C2
(d)
South West
North East
D1
D2
(e)
South
North
E1
E2
km/s
Shear velocity

Figure 3: Shear velocity vs depth along lines (a) A1-A2, (b) B1-B2, (c) C1-C2, (d) D1-D2, (e) E1-E2 from the joint inversion of receiver function and surface wave data. 1-D models from stations within 50 km of the line of section are interpolated to make the cross-sections. Grey areas indicate areas with no station coverage. Green triangles mark the location of stations. Topography along the line of section is plotted above. Labelled velocity anomalies 1-8 are discussed in the text.

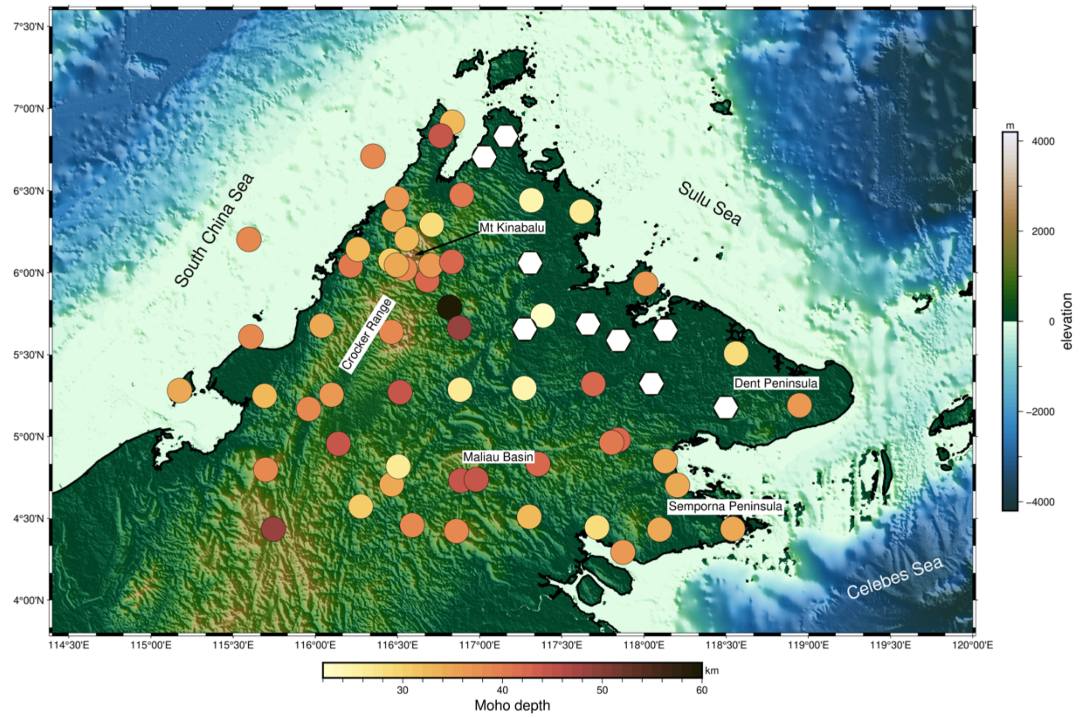

Figure 4: Moho depths at seismometer stations in Sabah picked from 1D shear velocity models from the joint inversion of receiver function and surface wave data. The colour of the circle indicated Moho depth for the station located at that point, as shown in the scale. White hexagons are locations where there was no clear Moho to be picked or where there were multiple plausible velocity discontinuities that could be the Moho.

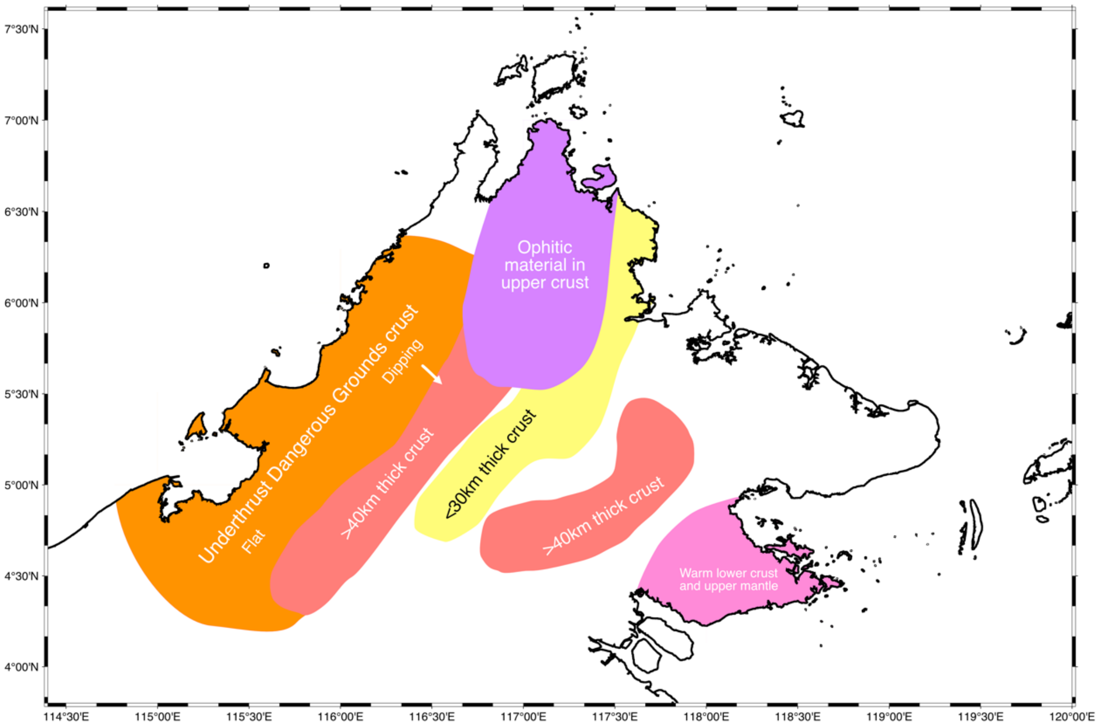

Figure 5: Summary map highlighting the key interpretations from this study from the shear velocity models derived from the joint inversion of receiver function and surface wave data.

Supplementary Material

Supplementary table 1: The name, instrument type, and location of the seismometers used in this study, together with the number of good receiver functions after quality control, and the crustal thickness estimated from the joint inversion of receiver function and surface wave data. Where the crustal thickness is N/A this is because there were no good receiver functions for that station. Where crustal thickness is 'X' these are stations where it was not possible to estimate the crustal thickness from the velocity model.

Network	Station	Instrument type	Latitude (N)	Longitude (E)	# of receiver functions	Crustal thickness (km)
YC	SBA2	3ESP	4.43506	115.74560	76	48
YC	SBA3	6TD	4.57347	116.27660	74	30
YC	SBA4	3ESP	4.45879	116.58977	73	38
YC	SBA5	6TD	4.42271	116.85881	84	38
YC	SBA6	3ESP	4.51025	117.30176	18	32
YC	SBA7	6TD	4.44587	117.71442	55	28
YC	SBA8	3ESP	4.43208	118.09522	183	34
YC	SBA9	6TD	4.43637	118.53992	76	34
YC	SBB2	6TD	4.79788	115.69913	62	38
YC	SBB3	3ESP	4.95640	116.14096	126	44
YC	SBB4	6TD	4.81717	116.50497	49	26
YC	SBB5	6TD	4.73101	116.88574	82	44
YC	MALB	3ESP	4.73740	116.97997	56	44
YC	SBB6	6TD	4.83194	117.35575	56	42
YC	SBB7	3ESP	4.96355	117.80282	70	40
YC	SBB8	6TD	4.85014	118.12941	79	34
YC	SBC1	6TD	5.28108	115.17476	24	34
YC	SBC2	3ESP	5.24880	115.69165	114	32
YC	SBC3	6TD	5.25540	116.09856	60	36
YC	SBC4	3ESP	5.27107	116.51573	76	44

YC	SBC5	6TD	5.28637	116.88076	73	26
YC	SBC6	3ESP	5.29518	117.27165	19	24
YC	SBC7	6TD	5.32075	117.69134	23	42
YC	SBC8	3ESP	5.32373	118.04523	16	X
YC	SBC9	3ESP	5.19098	118.94610	54	36
YC	SBD1	6TD	5.60898	115.60830	44	38
YC	SBD2	3ESP	5.67735	116.03960	55	34
YC	SBD3	6TD	5.63900	116.46225	89	38
YC	SBD4	3ESP	5.66416	116.87691	86	48
YC	SBD5	6TD	5.65637	117.27355	28	X
YC	SBD6	3ESP	5.68750	117.65900	28	X
YC	SBD7	6TD	5.64967	118.12955	80	X
YC	SBD8	6TD	5.50699	118.56041	34	28
YC	SBE1	6TD	6.20282	115.5963	33	38
YC	SBE2	6TD	6.04611	116.49462	83	34
YC	KINA	6TD	6.05826	116.56593	0	N/A
YC	SBE3	6TD	6.06708	116.83097	63	42
YC	SBE4	3ESP	6.05975	117.30715	48	X
YC	SBE5	6TD	5.93328	118.01012	37	36
YC	SBF1	6TD	6.45216	116.49845	48	36
YC	SBF2	3ESP	6.47376	116.89069	42	40
YC	SBF3	6TD	6.44177	117.31431	95	24
YC	SBF4	6TD	6.37312	117.62083	35	26
YC	SBG1	6TD	6.70950	116.35092	24	38
YC	SBG2	6TD	6.83352	116.76262	49	44
YC	SBG3	3ESP	6.83170	117.15904	55	X
MY	DVM	STS-2.5	4.98038	117.84421	18	42
MY	FSM	STS-2.5	5.085917	118.062783	0	N/A
MY	KAM	STS-2.5	6.0745	116.4583	49	30

MY	KDM	SS-1 Ranger	6.9167	116.8333	7	32
MY	KIM	STS-2.5	5.587083	117.844717	52	X
MY	KKM	STS-2	6.0443	116.2147	62	40
MY	KNM	STS-2.5	4.7026	118.203	86	34
MY	KPM	STS-2.5	6.0227	116.545417	26	38
MY	LDM	STS-2.5	5.1777	118.498	41	X
MY	MTM	STS-2.5	5.789333	116.81665	47	60
MY	PRM	STS-2.5	6.0455	116.70375	65	36
MY	PTM	STS-2.5	6.70523	117.0283	43	X
MY	RAM	STS-2.5	5.9546	116.681	70	42
MY	SDM	SS-1 Ranger	5.6409	117.195	0	N/A
MY	SGM	STS-2.5	5.03711	118.34795	0	N/A
MY	SMM	SS1-Ranger	4.439838	118.622028	0	N/A
MY	SPM	STS-2	4.7083	116.465	13	34
MY	SRM	STS-2.5	6.29265	116.708383	48	28
MY	SYM	STS-2.5	6.20585	116.5559	55	32
MY	TLM	STS-2.5	5.7391	117.385	26	22
MY	TNM	STS-2.5	5.168633	115.960183	38	38
MY	TPM	STS-2.5	6.1427	116.2596	23	32
MY	TSM	SS-1 Ranger	4.2936	117.8725	5	36
MY	WRM	STS-2.5	6.3229	116.47825	35	34

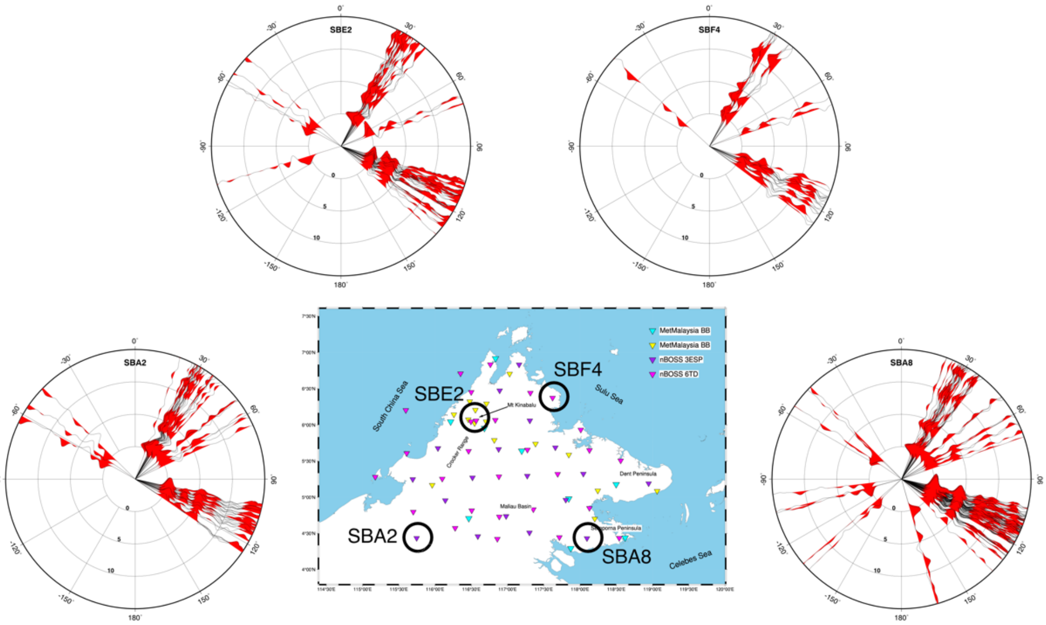

Supplementary figure 1: Examples of the receiver functions of individual events used in the station stacks for four stations across Sabah: SBA2, SBE2, SBF4, and SBA9, and a map indicating the station locations. Receiver functions are plotted with respect to backazimuth with positive amplitudes filled red.

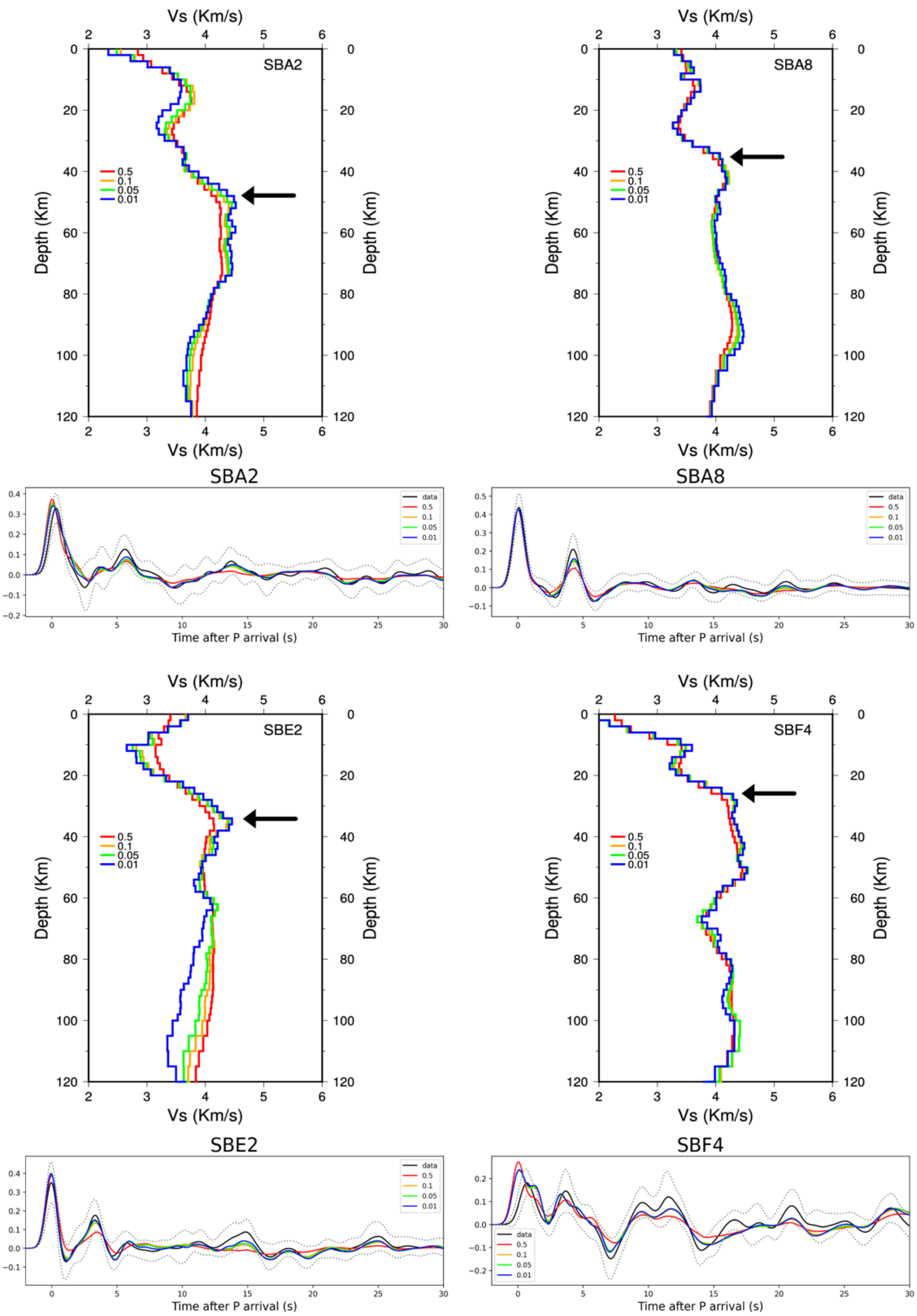

Supplementary figure 2: Examples of models of shear velocity vs depth from the joint inversion of surface wave and receiver function data, and the receiver functions for these models for four stations across Sabah: SBA2, SBE2, SBF4, and SBA9On each of the shear velocity and receiver function plots the coloured lines show the results from testing different weights of receiver function and surface wave data. On the shear velocity plots, the black arrow indicates the depth that is picked for the Moho in each example. On the receiver function plots, the receiver function data are shown in black.

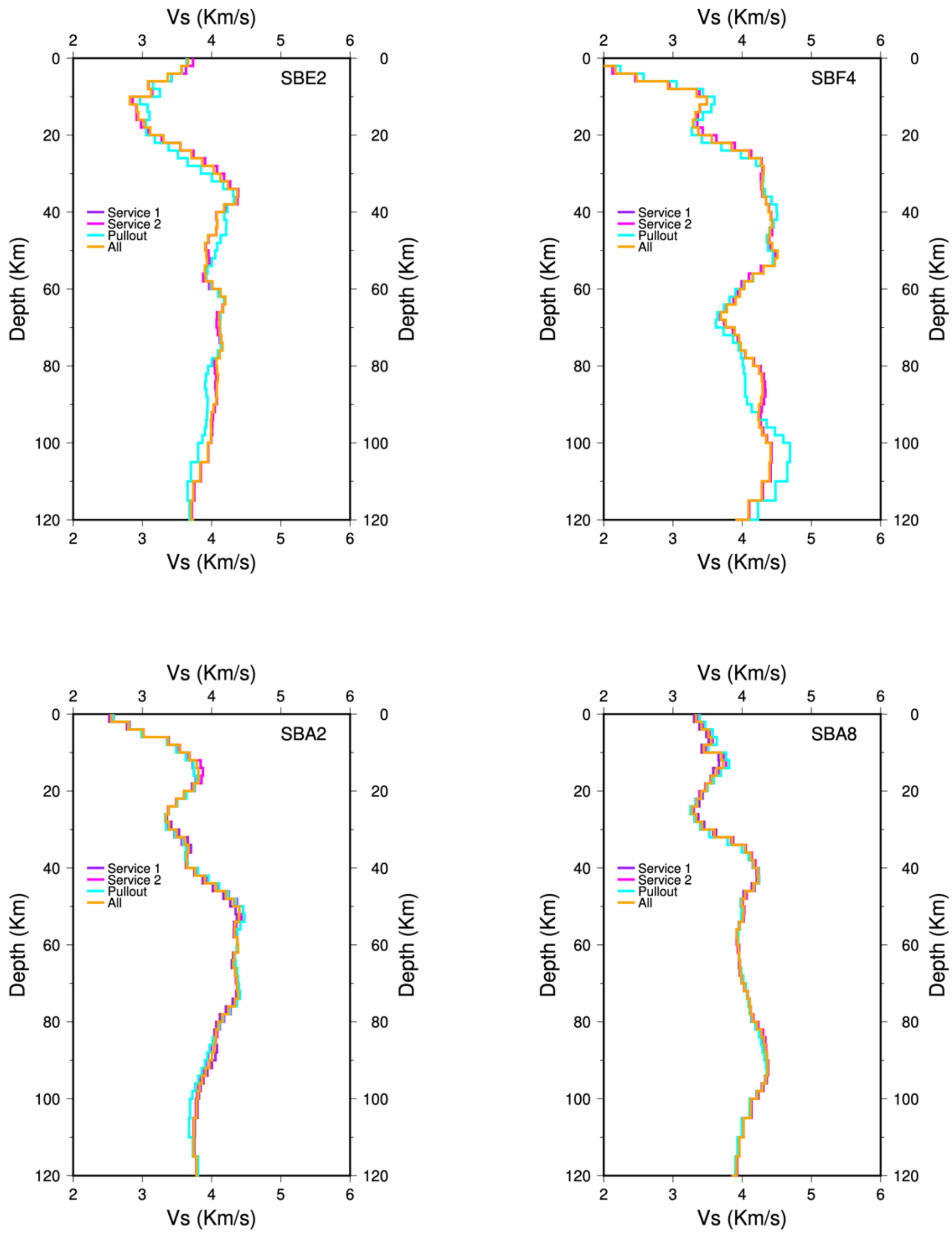

Supplementary figure 3: Examples of models of shear velocity vs depth from the joint inversion of surface wave and receiver function data four stations SBA2, SBE2, SBF4, and SBA9 with a p value of 0.1. On each shear velocity model the coloured lines show the different models that result from testing different subsets of the receiver function data: Service 1 (purple) is from the inversion of stacked receiver functions for events between March 2018-Sept 2018, Service 2 (magenta) is from the inversion of stacked receiver functions from events between Sept 2018-March 2019, Pullout is from the inversion of stacked receiver functions from events between March 2019-Jan 2020, and All is from the inversion of stacked receiver functions for the whole time period, as shown in Supplementary figure 1. For each station, the same surface wave dispersion data was used for each of the inversions.

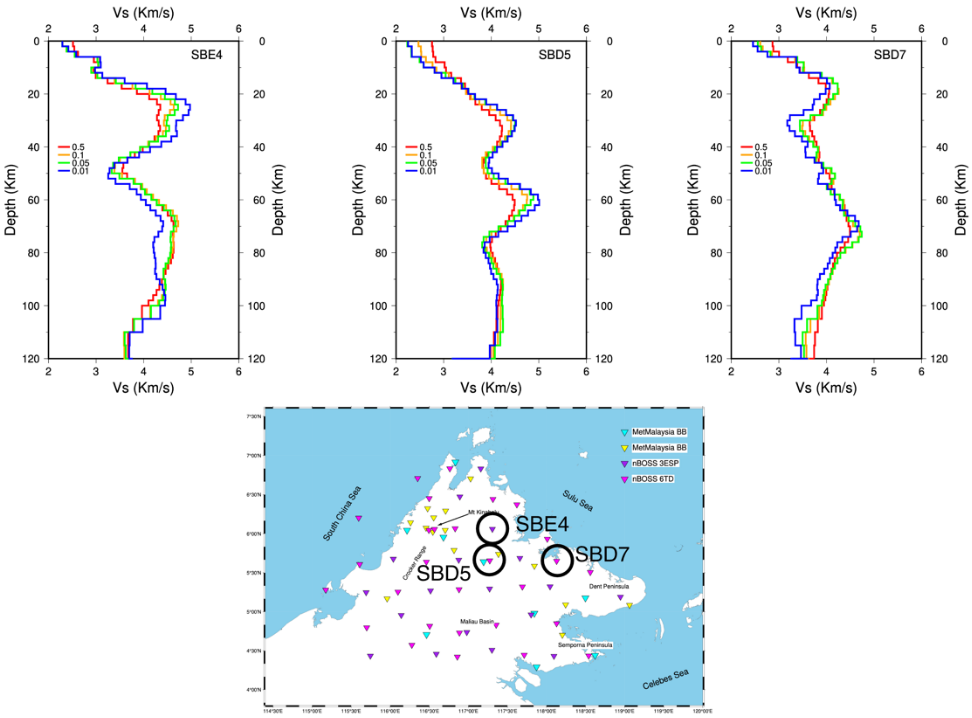

Supplementary figure 4: Examples of models of shear velocity vs depth from the joint inversion of surface wave and receiver function data for stations where a Moho was challenging to identify in this study. SBE4 and SBD5 are examples of stations with two potential discontinuities, while SBD7 shows a gradual increase in velocities over a wide depth range. On each shear velocity model the coloured lines show the different models that result from testing different weights of receiver function and surface wave data.

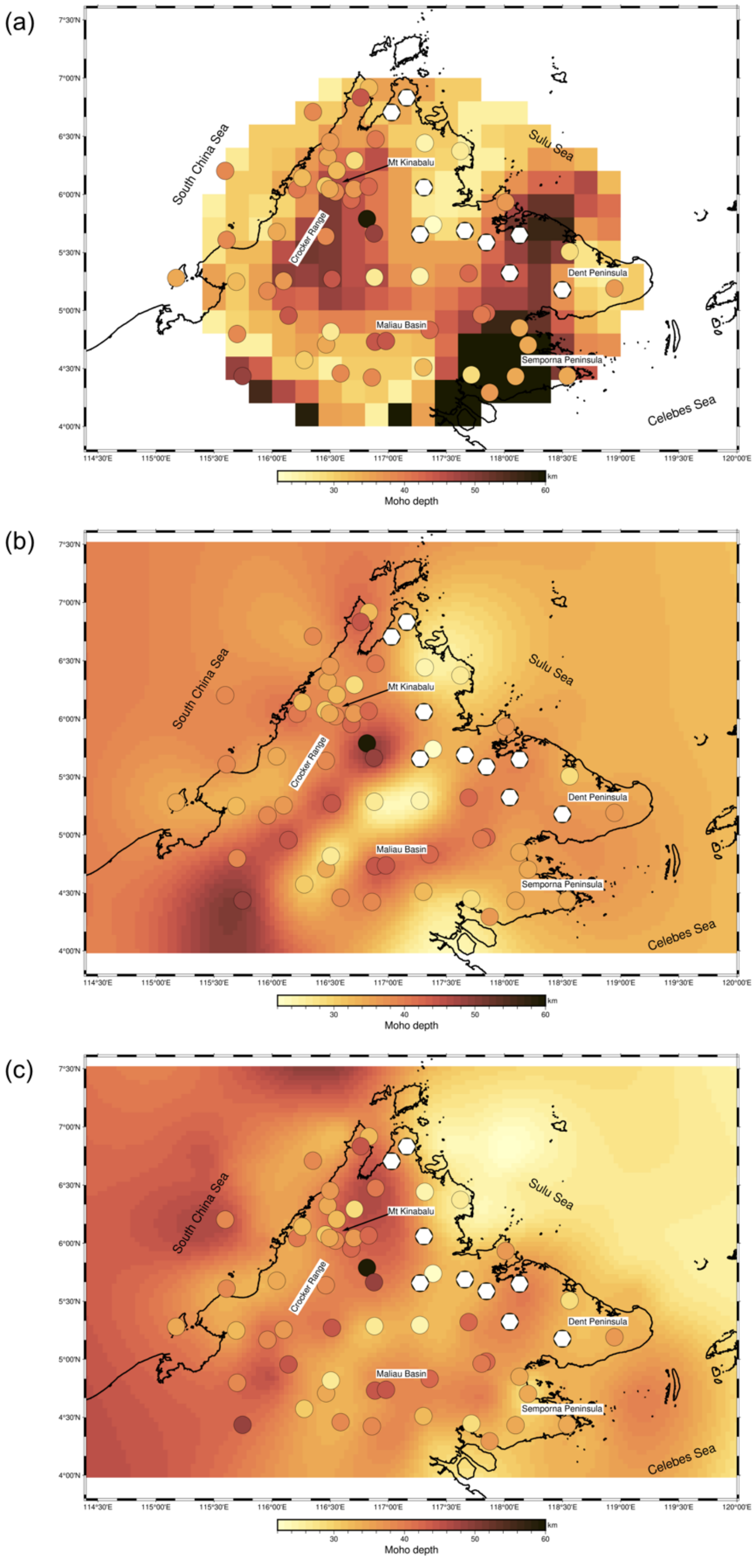

Supplementary figure 5: Comparison of Moho depths from this study (circles) with other Moho depth estimates from other studies of the region. (a) comparison with the Moho depth from Greenfield et al., (2022) based on the 4.1km/s velocity contour in their shear velocity model, (b) comparison with the Moho depth from Linang et al, (2022) from the interpolation of crustal depths obtained from stacked VDSS traces, assuming the depths reflect the Moho beneath stations, (c) comparison with the Moho depth from Linang et al,

(2022) from the interpolation of crustal depths at reflection points in the VDSS method.